Mineralogical Magazine, June 2013, Vol. 77(3), pp. 453–465

Camaronesite, $[Fe^{3+}(H_2O)_2(PO_3OH)]_2(SO_4)\cdot 1-2H_2O$, a new phosphate-sulfate from the Camarones Valley, Chile, structurally related to taranakite

A. R. KAMPF[1,*], S. J. MILLS[2], B. P. NASH[3], R. M. HOUSLEY[4], G. R. ROSSMAN[4] AND M. DINI[5]

[1] Mineral Sciences Department, Natural History Museum of Los Angeles County, 900 Exposition Boulevard, Los Angeles, CA 90007, USA
[2] Geosciences, Museum Victoria, GPO Box 666, Melbourne 3001, Australia
[3] Department of Geology and Geophysics, University of Utah, Salt Lake City, Utah 84112, USA
[4] Division of Geological and Planetary Sciences, California Institute of Technology, Pasadena, California 91125, USA
[5] Pasaje San Agustin 4045, La Serena, Chile

[*Received 25 April 2013; Accepted 25 April 2013; AE: G.D. Gatta*]

ABSTRACT

Camaronesite (IMA 2012-094), $[Fe^{3+}(H_2O)_2(PO_3OH)]_2(SO_4)\cdot 1-2H_2O$, is a new mineral from near the village of Cuya in the Camarones Valley, Arica Province, Chile. The mineral is a low-temperature, secondary mineral occurring in a sulfate assemblage with anhydrite, botryogen, chalcanthite, copiapite, halotrichite, hexahydrite, hydroniumjarosite, pyrite, römerite, rozenite and szomolnokite. Lavender-coloured crystals up to several mm across form dense intergrowths. More rarely crystals occur as drusy aggregates of tablets up to 0.5 mm in diameter and 0.02 mm thick. Tablets are flattened on {001} and exhibit the forms {001}, {104}, {015} and {018}. The mineral is transparent with white streak and vitreous lustre. The Mohs hardness is 2½, the tenacity is brittle and the fracture is irregular, conchoidal and stepped. Camaronesite has one perfect cleavage on {001}. The measured and calculated densities are 2.43(1) and 2.383 g/cm^3, respectively. The mineral is optically uniaxial (+) with $\omega = 1.612(1)$ and $\varepsilon = 1.621(1)$ (white light). The pleochroism is *O* (pale lavender) > *E* (colourless). Electron-microprobe analyses provided Fe_2O_3 31.84, P_2O_5 29.22, SO_3 15.74, H_2O 23.94 (based on O analyses), total 100.74 wt.%. The empirical formula (based on 2 P a.p.f.u.) is: $Fe_{1.94}(PO_3OH)_2(S_{0.96}O_4)(H_2O)_4\cdot 1.46H_2O$. The mineral is slowly soluble in concentrated HCl and extremely slowly soluble in concentrated H_2SO_4. Camaronesite is trigonal, *R*32, with cell parameters: $a = 9.0833(5)$, $c = 42.944(3)$ Å, $V = 3068.5(3)$ Å^3 and $Z = 9$. The eight strongest lines in the X-ray powder diffraction pattern are [d_{obs} Å(*I*)(*hkl*)]: 7.74(45)(101), 7.415(100)(012), 4.545(72)(110), 4.426(26)(018), 3.862(32)(021,202,116), 3.298(93)(027,119), 3.179(25)(208) and 2.818(25)(1·1·12,125). In the structure of camaronesite ($R_1 = 2.28\%$ for 1138 $F_o > 4\sigma F$), three types of Fe octahedra are linked by corner sharing with (PO_3OH) tetrahedra to form polyhedral layers perpendicular to *c* with composition $[Fe^{3+}(H_2O)_2(PO_3OH)]$. Two such layers are joined through SO_4 tetrahedra (in two half-occupied orientations) to form thick slabs of composition $[Fe^{3+}(H_2O)_2(PO_3OH)]_2(SO_4)$. Between the slabs are partially occupied H_2O groups. The only linkages between the slabs are hydrogen bonds. The most distinctive component in the structure consists of two Fe octahedra linked to one another by three PO_4 tetrahedra yielding an $[Fe_2(PO_4)_3]$ unit. This unit is also the key component in the sodium super-ionic conductor (NASICON) structure and has been referred to as the lantern unit. The polyhedral layers in the structure of camaronesite are similar to those in the structure of taranakite. The Raman spectrum exhibits peaks consistent with sulfate, phosphate, water and OH groups.

* E-mail: akampf@nhm.org
DOI: 10.1180/minmag.2013.077.4.05

Keywords: camaronesite, new mineral, sulfate, phosphate, Raman spectroscopy, crystal structure, taranakite, NASCION, Camarones Valley, Chile.

Introduction

The narrow, steep-walled Camarones Valley in Chile's Arica Province is known locally for its small-scale sulfate outcrops, which have been exploited in the past as small quarries and diggings (Salas, 1964, 1965). In late 2011, while searching the valley floor for rocks that had tumbled down from outcrops on the steep valley walls, Arturo Molina encountered a small boulder with unusual sulfate mineralization. This boulder yielded a variety of rare sulfates, including massive intergrowths of crystals of the new mineral described herein. On a second visit in early 2012, Molina found a second small boulder about 100 m west of the first discovery. This boulder contained vugs bearing free-standing crystals of the new mineral.

The new mineral species, a remarkable ferric iron phosphate–sulfate, is named camaronesite (kæm a:r 'oun æz ait) for the locality. In spite of the abundance of Fe, S and P in the natural environment, only two minerals, destinezite, and its amorphous analogue, diadochite, are known, with only these cations (Peacor *et al*., 1999; Mills *et al*., 2012). Several other minerals contain phosphate and sulfate ions; however, many of these minerals are members of the alunite supergroup (Mills *et al*., 2009; Bayliss *et al*., 2010) or complex white Al phosphate–sulfates such as peisleyite (Mills *et al*., 2011), sanjuanite (Colombo *et al*., 2011), hotsonite (Beukes *et al*., 1984), kribergite (de Bruiyn *et al*., 1989) and sasaite (Martini, 1978).

The new mineral and name have been approved by the Commission on New Minerals, Nomenclature and Classification of the International Mineralogical Association (IMA 2012-094). The description of the new mineral was based on five specimens, which are all designated as cotype specimens and are deposited in the Natural History Museum of Los Angeles County, 900 Exposition Boulevard, Los Angeles, California 90007, USA under catalogue numbers 64023, 64024, 64025, 64026 and 64027. Specimens 64023–64026 are from the first boulder found. Specimen 64027 is from the second boulder.

Occurrence and paragenesis

The location where Arturo Molina found the two boulders is ~9 km NE of the village of Cuya in the Camarones Valley, Arica Province, Chile. The small boulders evidently originated from a leached outcrop located approximately at 19º5′58″S 70º7′6″W, high on the NW side of the steep valley, directly above the place where the boulders were found. We have designated the site of the deposit as the Cuya NE9 sulfate occurrence to differentiate it from other sulfate deposits at different distances from Cuya, as well as from other deposits with different mineral assemblages. Note that we are also investigating several potentially new minerals from a nearby deposit rich in arsenite minerals, which is also ~9 km NE of Cuya. This site will be designated the Cuya NE9 arsenite occurrence. Using this same approach, the chloride-rich deposit in the Camarones Valley 5 km NE of Cuya, at which a recent new Mg-rich mineral related to paratacamite (IMA-2013-014) was found, is designated the Cuya NE5 chloride occurrence.

The rocks in the Camarones Valley area consist of faulted and metamorphosed lavas, lithic tuffs and marine sediments. Sulfide accumulations (pyrite with lesser arsenopyrite, sphalerite, etc.) in the marine sediments (shales and sandstones) have been oxidized under increasingly arid conditions, yielding extensive suites of secondary sulfates, arsenates, arsenites, chlorides, etc. (Salas, 1964, 1965).

The first of the two small boulders in which the camaronesite was found measured roughly 25 cm × 20 cm × 15 cm and weighed ~8 kg. The second boulder measured ~35 cm × 30 cm × 30 cm and weighed ~20 kg. Both boulders had crudely zoned structures with yellow-brown limonitic exterior coatings followed by the sulfate assemblages and then sulfide-rich cores. The first boulder consisted of a dense intergrowth of minerals with few, if any, vugs. The second boulder contained numerous vugs containing well formed crystals of several of the sulfate minerals, most notably camaronesite and copiapite.

The sulfate assemblage in the first boulder included anhydrite, botryogen, camaronesite, chalcanthite, copiapite, halotrichite, hexahydrite, römerite, rozenite and szomolnokite. Its core contained prominent patches and small crystals of unaltered pyrite and a lesser amount of arsenopyrite. The sulfate assemblage in the second boulder included anhydrite, camaronesite,

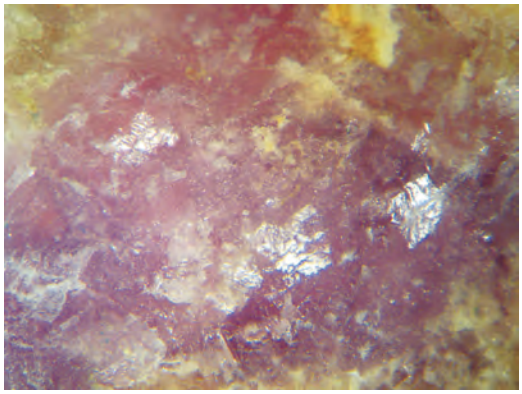

FIG. 1. Dense intergrowth of camaronesite and anhydrite. Note reflections from cleavages on broken camaronesite crystals (field of view = 7 mm).

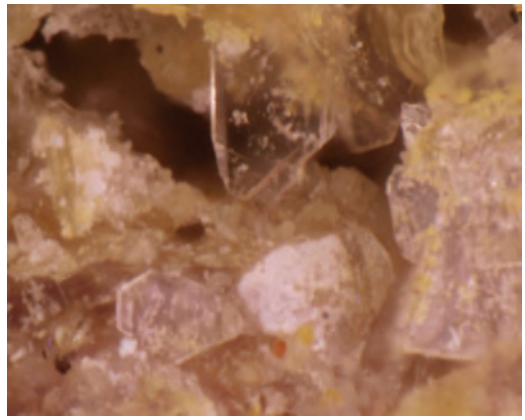

FIG. 2. Tabular pink camaronesite crystals with yellow copiapite (field of view = 7 mm).

chalcanthite, copiapite, hydroniumjarosite, rozenite and szomolnokite. Its core was richer in sulfides than that of the first boulder, pyrite being most prominent with lesser amounts of arsenopyrite, chalcopyrite and sphalerite. Chunks of actinolite, assumed to be remnants of the metamorphosed shale, were also a minor component of the second boulder. The small boulders evidently were sulfide accumulations in the metamorphosed shale that altered from the outside inwards.

Physical and optical properties

Crystals of camaronesite usually occur in lavender-coloured, dense intergrowths, often heavily included by anhydrite. On broken surfaces of these intergrowths, cleavage planes up to several mm across can be observed (Fig. 1). More rarely crystals occur as pink to pale lavender tablets up to 0.5 mm in diameter and 0.02 mm thick forming isolated crystals (Fig. 2) or drusy aggregates lining vughs and seams. Tabular crystals (on specimen 64027) are flattened on {001} and exhibit the forms {001}, {104}, {015} and {018} (Fig. 3). No evidence of twinning was observed morphologically, optically or by X-ray diffraction (XRD).

Camaronesite has a white streak. It is transparent and has vitreous lustre. It does not fluoresce in long or short wave ultraviolet light. The Mohs hardness is 2½, based on scratch tests with gypsum and calcite. The tenacity is brittle and the fracture is irregular, conchoidal and stepped. The mineral exhibits one perfect cleavage on {001}. The density measured by floatation in an aqueous solution of sodium polytungstate is 2.43(1) g/cm^3, but because crystals generally contain inclusions of anhydrite, this value is probably too high. The calculated density is 2.383 g/cm^3, based on the empirical formula and the unit cell determined by single-crystal XRD. A small crystal of camaronesite requires several hours to dissolve in cold, concentrated HCl and several days to dissolve in concentrated H_2SO_4.

Optically, camaronesite is uniaxial positive, with ω = 1.612(1), ε = 1.621(1), measured in white light. The mineral is pleochroic: *O* (pale lavender) > *E* (colourless).

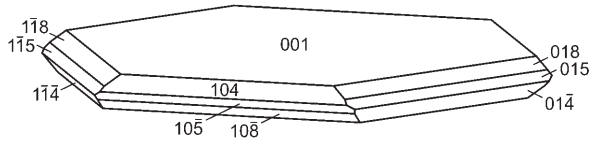

FIG. 3. Crystal drawing of camaronesite crystal, clinographic projection.

Raman spectroscopy

Raman spectroscopic micro-analyses were obtained using a Renishaw M1000 micro-Raman spectrometer system. Light from a 514.5 nm argon laser was focused onto the sample with a 100× objective lens, and at 100% power could provide ~5 mW of power at the sample, in a spot size of ~1 μm. Peak positions were periodically calibrated against a silicon standard and rarely varied more than 1 cm^{-1}. All spectra were obtained with a dual-wedge polarization scrambler inserted directly above the objective lens to minimize the effects of polarization.

The camaronesite Raman spectrum (Fig. 4) was obtained from an ~76 μm × 55 μm grain in a polished microprobe section. It shows a strong, broad OH-stretching band running from ~3600 to 2800 cm^{-1} with possible components near 3463, 3363 and 3140 cm^{-1}. Evidence for molecular water comes from a narrower H_2O-bending region centred at ~1610 cm^{-1} with likely components at ~1638 and 1596 cm^{-1}. The spectrum also shows strong, sharp bands at 1014, 1080 and 937 cm^{-1} that are in a position where both PO_4^{3-} and SO_4^{2-} vibrations occur. Curve fitting indicates that additional bands appear at 526, 305, 254 and 227 cm^{-1}.

The Raman frequencies of the free phosphate ion tend to occur at somewhat lower energies than those of the free sulfate ion (table II-6e in Nakamoto, 1978). However, an examination of the Raman spectra of hydrated ferric sulfate and phosphate minerals on the RRUFF website (Downs, 2006) shows that phosphate bands in the 1000 cm^{-1} region can be at nearly the same, or occasionally, slightly higher energies than the sulfate bands depending on the specific phase. Thus, while it is reasonable to assign the dominant bands in the 1100–950 cm^{-1} region to the ν_1 tetrahedral TO_4 vibrations (T = P or S), we cannot reliably assign the individual bands to either phosphate or sulfate with the available data.

Chemical composition

Ten chemical analyses, eight on crystals from the first boulder (specimens 64023–64026) and two on crystals from the second boulder (specimen 64027), were performed at the University of Utah using a Cameca SX-50 electron microprobe (EMP) with four wavelength dispersive spectrometers. Analytical conditions were 15 kV accelerating voltage, 10 nA beam current and a beam diameter of 20 μm. Counting times were 20 s on peak and 10 s on + and − background. No other elements were detected by energy dispersive spectroscopy. Other likely elements were sought by electron microprobe analysis, but none was found to be above the limit of detection. Raw X-ray intensities were corrected for matrix effects with a $\phi(\rho z)$ algorithm (Pouchou and Pichoir, 1991).

CHN analyses of the dense crystal intergrowths provided H_2O values that were about half of those expected. These same intergrowths provided densities measured by Berman balance in the 2.6–2.7 g cm^{-3} range. Examination by powder XRD and polarized-light microscopy showed

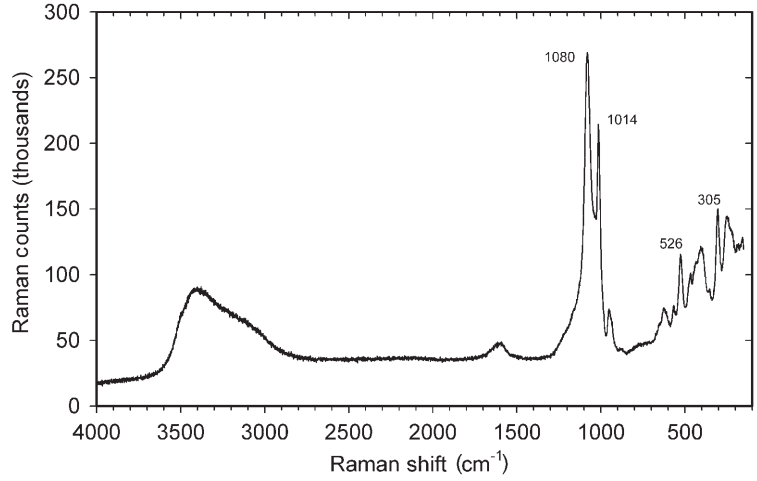

FIG. 4. Raman spectrum of camaronesite.

these crystals of camaronesite to contain numerous inclusions of anhydrite, thus accounting for the discrepancies in the H_2O content and density. The drusy camaronesite crystals contain far fewer inclusions and a CHN analysis on a 2.8 mg sample of this material provided an H_2O content of 20.29 wt.%, only ~3 wt.% lower than that indicated by the structure determination and EMP oxygen analyses. Due to the problem with the CHN analyses caused by inclusions, we ultimately chose to report the H_2O contents in camaronesite based upon careful EMP analyses of O (determined from the difference between measured and stoichiometric oxygen; see Nash, 1992), which closely match the amount of H_2O provided by the structure determination. It is also worth noting that the CHN analyses confirmed that the C and N contents of camaronesite are negligible. Analytical data are given in Table 1.

The empirical formula (based on 2 P a.p.f.u.) is $Fe_{1.94}(PO_3OH)_2(S_{0.96}O_4)(H_2O)_4 \cdot 1.46H_2O$. The simplified formula is $Fe_2^{3+}(PO_3OH)_2(SO_4)(H_2O)_4 \cdot 1{-}2\ H_2O$. It should be noted that the H_2O range in the analyses corresponds to 0.88–2.08 non-structural H_2O p.f.u. in the empirical formula. The two EMP analyses on free-standing crystals from the second boulder provided analytical values for all components within the ranges obtained for the massive crystals from the first boulder, although the H_2O values for the free-standing crystals fell towards the lower end of the range. The free-standing crystals analysed contained approximately one non-structural H_2O group p.f.u.

The Gladstone-Dale compatibility index $1 - (K_P/K_C)$ is 0.012 for the empirical formula, indicating superior compatibility (Mandarino, 2007).

X-ray crystallography and structure refinement

Both powder and single-crystal X-ray studies were carried out using a Rigaku R-Axis Rapid II curved imaging plate microdiffractometer, with monochromatized Mo$K\alpha$ radiation. For the powder-diffraction study, observed d spacings and intensities were derived by profile fitting using *JADE 2010* software (Materials Data, Inc.). The powder data presented in Table 2 show good agreement with the pattern calculated from the structure determination. Unit-cell parameters refined from the powder data using *JADE 2010* with whole-pattern fitting are: a = 9.0679(10), c = 42.991(6) Å, and V = 3061.4(6) Å^3.

For the crystal-structure study, the best refinement was obtained on a cleavage fragment carefully selected from intergrown camaronesite crystals from specimen 64023 (which originated from the first boulder). The Rigaku *CrystalClear* software package was used for processing the structure data, including the application of an empirical multi-scan absorption correction using *ABSCOR* (Higashi, 2001). The structure was solved in the trigonal $R32$ space group by direct methods using *SIR2004* (Burla *et al*., 2005). *SHELXL-97* (Sheldrick, 2008) was used for the refinement of the structure. No unindexed or streaked diffraction spots were observed and there were no space group violations. The Flack parameter, 0.04(2), suggests the absence of racemic twinning.

The SO_4 group was found to consist of two half-occupied tetrahedral groups sharing a common base, such that the O atoms of the base (two O5 and one O6) are fully occupied and the apical O atom (O7) and the S atom are half

TABLE 1. Analytical data for camaronesite.

Constituent	Wt.%	Range	SD	Ideal wt.% (1 H_2O p.f.u.)	Ideal wt.% (2 H_2O p.f.u.)	Standard
Fe_2O_3	31.84	30.53–32.54	0.75	32.60	31.45	hematite
P_2O_5	29.22	28.19–31.28	1.01	28.98	27.95	apatite
SO_3	15.74	15.27–16.32	0.34	16.35	15.77	baryte
O	(56.76)	55.17–57.80	0.93			hematite
H_2O*	23.94	21.75–25.64	1.43	22.07	24.83	
Total	100.74			100	100	

* Based on EMP oxygen analyses (Nash, 1992).

TABLE 2. Powder X-ray data for camaronesite.

I_{obs}	d_{obs}	d_{calc}	I_{calc}	*h k l*
24	14.49(6)	14.3147	22	003
45	7.74(3)	7.7376	48	101
100	7.415(18)	7.3863	100	012
		7.1573	4	006
15	5.818(13)	5.8010	17	015
12	4.853(11)	4.8376	13	107
72	4.545(7)	4.5417	69	110
26	4.426(14)	4.4340	29	018
		4.3290	2	113
		3.9168	5	021
32	3.862(4)	3.8688	9	202
		3.8348	15	116
		3.7693	2	1·0·10
		3.5787	5	0·0·12
9	3.586(7)	3.5760	2	205
		3.3111	11	027
93	3.298(2)	3.2897	87	119
25	3.179(4)	3.1727	28	208
		2.9661	2	211
13	2.945(10)	2.9451	13	122
18	2.900(10)	2.9005	18	0·2·10
		2.8654	3	214
		2.8109	16	1·1·12
25	2.818(9)	2.8096	15	125
19	2.781(9)	2.7708	18	2·0·11
12	2.676(4)	2.6756	14	217
		2.6221	3	300
		2.6009	15	128
24	2.595(2)	2.5792	11	033
		2.4445	4	2·1·10
6	2.436(4)	2.4219	3	1·1·15
		2.4188	2	2·0·14
3	2.369(7)	2.3654	5	1·2·11
		2.2980	4	309
5	2.285(6)	2.2708	5	220
2	2.249(13)	2.2428	2	223
		2.1789	3	131
10	2.170(3)	2.1706	5	312
		2.1645	4	226
		2.1380	2	134
9	2.129(3)	2.1349	4	1·2·14
		2.1255	3	2·0·17
		2.1151	2	3·0·12
7	2.047(5)	2.0505	3	229
		2.0450	4	0·0·21
9	2.020(8)	2.0212	12	318
3	1.994(15)	1.9923	4	2·1·16
		1.9645	2	401
5	1.959(7)	1.9597	2	0·2·19
		1.9451	4	1·3·10
13	1.930(5)	1.9251	12	1·2·17
5	1.909(8)	1.9045	6	3·1·11
2	1.871(6)	1.8647	3	1·1·21
		1.8205	2	1·3·13
20	1.802(14)	1.7993	15	2·1·19
		1.7983	3	232
3	1.775(9)	1.7779	3	3·1·14
		1.7661	2	235
20	1.7127(10)	1.7166	11	410
		1.7106	8	238
		1.7044	3	143
		1.6637	2	3·2·10
10	1.6528(13)	1.6556	2	0·4·14
		1.6512	7	3·1·17
		1.6381	2	2·3·11
7	1.6170(16)	1.6152	6	4 1 9
		1.5863	2	4·0·16
13	1.5731(14)	1.5697	11	1·3·19
9	1.5539(18)	1.5554	3	2·3·14
		1.5518	5	0·4·17
		1.5477	2	4·1·12
		1.5139	4	330
12	1.5069(11)	1.5098	3	508
		1.5011	5	1·1·27
		1.4857	3	241
9	1.4846(17)	1.4836	3	4·0·19
		1.4831	2	422
2	1.442(7)	1.4430	3	339
3	1.430(5)	1.4289	3	0·2·28
		1.4186	2	3·1·23
5	1.4102(19)	1.4121	3	511
		1.4103	2	3·2·19
4	1.3909(18)	1.4048	2	2·4·10
		1.3893	2	4·2·11
8	1.3646(10)	1.3663	4	158
		1.3599	2	0·3·27

Only calculated lines with intensities of 2 or greater are listed.

occupied. Attempts to resolve the SO_4 group into separate fully occupied sites using lower symmetry (e.g. *C*2 and *P*1) and/or multiple cell lengths along **c** were unsuccessful.

Difference Fourier syntheses located the H atom sites associated with the $PO_3(OH)$ group and with the H_2O groups participating in Fe coordination. Three partially occupied non-structural H_2O sites (OW10, OW11 and OW12) were also located. The H atom sites associated with the partially occupied H_2O sites could not be located and because of the consequent uncertainty in

assigning hydrogen bonds from the non-structural H_2O groups, no corresponding bond-valence contributions are included in the bond-valence analysis. Note that possible hydrogen bonds from the non-structural H_2O groups based on O–O bond distances are as follows: OW10···OH4 (2.60, 2.68 Å), OW10···O7 (2.71 Å), OW10···OW9 (2.91 Å), OW11···OH4 (2.81 Å), OW11···OW8 (2.77, 2.79 Å), OW12···OH4 (2.86, 2.93 Å) and OW12···OW8 (2.78 Å).

In the final refinement, the Fe sites (Fe1, Fe2 and Fe3) and the S site refined to less than full occupancy, in close agreement with the empirical formula. The refined occupancies of the non-structural H_2O sites (OW10, OW11 and OW12) provided a total of 1.43 H_2O p.f.u.,approximately midway in the 0.88–2.08 range provided by the EMP analyses. Note that the rather large U_{eq} for OW12 suggests that its refined site occupancy might be somewhat too large.

The data collection and structure refinement details are provided in Table 3, atom coordinates and displacement parameters in Table 4, selected bond distances in Table 5 and bond-valence summations (BVS) in Table 6. Note that the rather low BVS for O6 and O7, both of which form unlinked vertices of the SO_4 group, suggest that they may have some OH character; this would serve to compensate for the charge deficiency created by the deficiencies in Fe and S noted above. Lists of observed and calculated structure factors have been deposited with the journal and can be downloaded from http://www.minersoc.org/pages/e_journals/dep_mat_mm.html.

Description of the structure

In the structure of camaronesite (Fig. 5), three types of Fe octahedra are linked by corner sharing with (PO_3OH) tetrahedra to form layers perpendicular to *c* with composition [$Fe^{3+}(H_2O)_2(PO_3OH)$]. Two adjacent opposite-facing layers are joined through SO_4 tetrahedra (in two half-

TABLE 3. Data collection and structure refinement details for camaronesite.

Diffractometer	Rigaku R-Axis Rapid II
X-ray radiation / power	Mo*K*α (λ = 0.71075 Å)/50 kV, 40 mA
Temperature	298(2) K
Structural Formula	$Fe^{3+}_{1.922}(PO_3OH)_2(S_{0.954}O_4)(H_2O)_4 \cdot 1.43H_2O$
Space group	*R*32
Unit-cell dimensions	*a* = 9.0833(5) Å
	c = 42.944(3) Å
V	3068.5(3) Å^3
Z	9
Density (for above formula)	2.395 g cm^{-3}
Absorption coefficient	2.526 mm^{-1}
F(000)	2228
Crystal size (μm)	130 × 100 × 10
θ range	3.21 to 25.01°
Index ranges	$-10 \leqslant h \leqslant 8$, $-10 \leqslant k \leqslant 10$, $-51 \leqslant l \leqslant 51$
Reflections collected / unique	7122 / 1215; R_{int} = 0.051
Reflections with $F_o > 4\sigma(F)$	1138
Completeness to θ = 25.01°	99.2%
Max. and min. transmission	0.9752 and 0.7348
Refinement method	Full-matrix least-squares on F^2
Parameters refined	154
GoF	1.052
Final *R* indices [$F_o > 4\sigma(F)$]	R_1 = 0.0228, wR_2 = 0.0492
R indices (all data)	R_1 = 0.0258, wR_2 = 0.0504
Flack parameter	0.04(2)
Largest diff. peak / hole	+0.381 / −0.298 *e*/A^3

$R_{int} = \Sigma|F_o^2 - F_o^2(\text{mean})|/\Sigma[F_o^2]$. GoF = $S = \{\Sigma[w(F_o^2 - F_c^2)^2]/(n-p)\}^{1/2}$. $R_1 = \Sigma||F_o| - |F_c||/\Sigma|F_o|$. $wR_2 = \{\Sigma[w(F_o^2 - F_c^2)^2]/\Sigma[w(F_o^2)^2]\}^{1/2}$; $w = 1/[\sigma^2(F_o^2) + (aP)^2 + bP]$ where *a* is 0.0156, *b* is 5.5806 and *P* is $[2F_c^2 + \text{Max}(F_o^2, 0)]/3$.

TABLE 4. Atom coordinates and displacement parameters (Å^2) for camaronesite.

	Occ.	*x*/*a*	*y*/*b*	*z*/*c*	U_{eq}	U_{11}	U_{22}	U_{33}	U_{23}	U_{13}	U_{12}
Fe1	0.961(4)	0.0000	0.0000	0.791134(15)	0.0115(3)	0.0128(3)	0.0128(3)	0.0088(4)	0.000	0.000	0.00641(16)
Fe2	0.963(4)	0.6667	0.3333	0.762764(16)	0.0135(3)	0.0148(3)	0.0148(3)	0.0110(4)	0.000	0.000	0.00741(16)
Fe3	0.959(4)	0.0000	0.0000	0.685115(16)	0.0145(3)	0.0171(3)	0.0171(3)	0.0094(4)	0.000	0.000	0.00853(16)
P	1	0.77108(11)	0.71492(11)	0.737440(19)	0.0166(2)	0.0206(5)	0.0138(4)	0.0137(4)	–0.0005(4)	0.0002(3)	0.0074(4)
S	0.477(4)	0.6943(2)	0.8045(2)	0.84165(3)	0.0161(6)	0.0171(12)	0.0187(10)	0.0123(11)	0.0051(7)	0.0047(8)	0.0087(8)
O1	1	0.8635(3)	0.7902(3)	0.70730(5)	0.0281(7)	0.0334(16)	0.0284(14)	0.0202(11)	0.0081(10)	0.0051(11)	0.0137(12)
O2	1	0.8779(3)	0.7905(3)	0.76631(5)	0.0240(6)	0.0308(16)	0.0220(12)	0.0183(11)	–0.0046(9)	–0.0034(12)	0.0125(13)
O3	1	0.7073(4)	0.5246(3)	0.73650(5)	0.0334(7)	0.0572(19)	0.0176(13)	0.0205(13)	–0.0013(10)	–0.0088(12)	0.0150(12)
OH4	1	0.6157(4)	0.7430(4)	0.73770(6)	0.0414(8)	0.0366(17)	0.061(2)	0.0360(16)	–0.0039(15)	–0.0016(14)	0.0313(16)
H4	1	0.554(5)	0.722(6)	0.7547(8)	0.050						
O5	1	0.7948(3)	0.9312(3)	0.81857(6)	0.0317(7)	0.0333(15)	0.0212(15)	0.0384(14)	0.0082(11)	0.0236(13)	0.0120(12)
O6	1	0.6667	0.6368(4)	0.8333	0.0449(11)	0.051(3)	0.0287(16)	0.062(3)	0.0121(12)	0.024(2)	0.0256(15)
O7	0.50	0.7928(7)	0.8796(11)	0.87049(11)	0.0514(17)	0.031(3)	0.075(5)	0.025(2)	0.002(3)	–0.003(2)	0.008(4)
OW8	1	0.8003(3)	0.9472(3)	0.65471(6)	0.0285(7)	0.0258(14)	0.0337(16)	0.0218(13)	0.0005(11)	–0.0044(12)	0.0117(13)
H8a	1	0.812(5)	0.962(4)	0.6343(6)	0.034						
H8b	1	0.719(4)	0.832(3)	0.6563(8)	0.034						
OW9	1	0.8569(4)	0.4890(4)	0.79238(6)	0.0329(7)	0.0300(17)	0.0267(16)	0.0328(16)	0.0013(13)	–0.0093(13)	0.0074(12)
H9a	1	0.909(5)	0.445(4)	0.8026(8)	0.039						
H9b	1	0.920(5)	0.600(3)	0.7900(10)	0.039						
OW10	0.281(9)	0.9086(15)	0.0258(14)	0.8888(2)	0.051(4)	0.057(9)	0.046(7)	0.043(7)	0.000(5)	0.000(5)	0.021(7)
OW11	0.203(14)	0.483(2)	0.653(3)	0.6573(4)	0.045(8)	0.045(12)	0.038(12)	0.046(15)	–0.019(11)	–0.003(8)	0.016(10)
OW12	0.230(16)	0.452(3)	0.759(3)	0.6444(5)	0.104(14)	0.063(13)	0.09(2)	0.107(17)	0.035(16)	–0.015(11)	0.005(12)

TABLE 5. Selected bond distances (Å) and angles (º) in camaronesite.

Fe1−O2(×3)	1.969(2)	P−O1	1.508(2)
Fe1−O5(×3)	2.022(2)	P−O2	1.511(2)
<Fe1−O>	2.001	P−O3	1.524(3)
		P−OH4	1.555(3)
Fe2−O3(×3)	1.946(2)	<P−O>	1.525
Fe2−OW9(×3)	2.039(3)		
<Fe2−O>	2.002	S−O5	1.436(3)
		S−O5	1.445(3)
Fe3−O1(×3)	1.927(2)	S−O6	1.459(4)
Fe3−OW8(×3)	2.087(2)	S−O7	1.479(5)
<Fe3−O>	2.023	<S−O>	1.455

Hydrogen bonds (D = donor, A = acceptor)

D−H		d(D−H)	d(H···A)	<DHA	d(D···A)	A	<HDH
OH4−H4		0.88(3)	1.82(3)	150(4)	2.617(6)	O7	
OW8−H8a		0.88(2)	2.24(3)	144(3)	3.002(4)	O3	
		0.88(2)	2.26(3)	131(3)	2.918(4)	O3	
OW8−H8b		0.93(3)	1.94(3)	150(3)	2.79(2)	OW11	102
		0.93(3)	1.98(3)	140(3)	2.79(2)	OW11	
		0.93(3)	2.23(3)	116(3)	2.78(2)	OW12	
OW9−H9a		0.87(2)	1.91(3)	163(4)	2.758(3)	O6	113
OW9−H9b		0.88(3)	2.20(3)	133(3)	2.867(4)	O2	

occupied orientations) to form thick slabs of composition $[Fe^{3+}(H_2O)_2(PO_3OH)]_2(SO_4)$. Partially occupied H_2O groups between the layers account for 1 to 2 H_2O p.f.u., yielding the complete formula $[Fe^{3+}(H_2O)_2(PO_3OH)]_2(SO_4)\cdot 1-2H_2O$. The only linkages between the

TABLE 6. Bond-valence analysis for camaronesite. Values are expressed in valence units.

	O1	O2	O3	OH4	O5	O6	O7	OW8	OW9	Σ
Fe1		0.54 × 3→			0.47 × 3→					3.03
Fe2			0.58 × 3→						0.45 × 3→	3.09
Fe3	0.61 × 3→							0.40 × 3→		3.03
P	1.30	1.29	1.24	1.14						4.97
S					1.59 × ½↓ 1.55 × ½↓	1.49	1.41			6.04
H4				0.77			0.23			1.00
H8a			0.12					0.88		1.00
H8b								0.82		1.00*
H9a						0.19			0.81	1.00
H9b		0.16							0.84	1.00
Σ	1.91	1.99	1.94	1.91	2.04	1.68	1.64	2.10	2.10	

Multiplicity is indicated by × →↓; P^{5+}−O bond strength from Brese and O'Keeffe (1991); Fe^{3+}−O and S^{6+}−O bond strengths from Brown and Altermatt (1985); the bond strengths are based on the refined site occupancies for the Fe1, Fe2, Fe3 and S sites; hydrogen-bond strengths based on O···O bond lengths, also from Brown and Altermatt (1985); OW10, OW11 and OW12 are not included.

* H8b hydrogen bonds to two partially occupied OW11 and one partially occupied OW12, with an estimated total bond strength of 0.18 v.u.

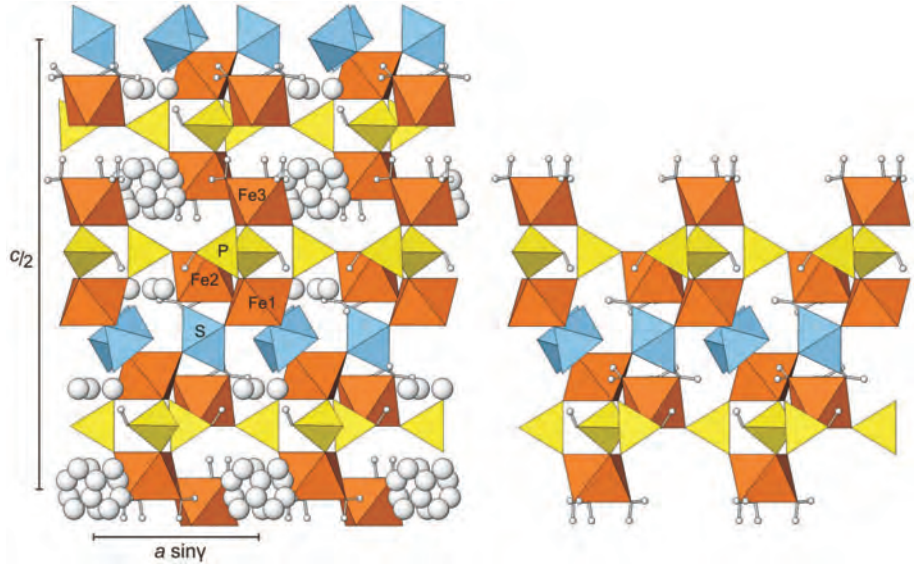

FIG. 5. The crystal structure of camaronesite. The image on the right shows a single polyhedral layer on edge. Partially occupied non-structural H_2O groups are large white spheres; H atoms are small white spheres. Note that the two half-occupied SO_4 groups share the same base and, therefore, look similar to an octahedron in this projection.

thick slabs are hydrogen bonds. The weak bonding between the slabs accounts for the perfect cleavage on {001}.

The Fe1 and Fe3 octahedra link to each other by sharing corners with three (PO_3OH) tetrahedra, thereby forming a distinctive [$Fe_2(PO_3OH)_3$] unit (Fig. 6), sometimes referred to as a 'lantern unit' because of its similarity in appearance to a lantern

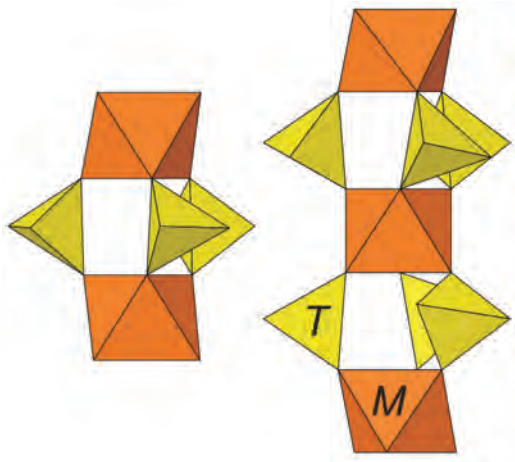

FIG. 6. [$M_2(TO_4)_3$] lantern unit (left) and [$M_3(TO_4)_6$] double lantern unit (right).

(see below). The Fe2 octahedron shares three adjacent corners with (PO_3OH) tetrahedra, each of which is part of a different [$Fe_2(PO_3OH)_3$] lantern unit. The Fe2 octahedron, thereby, serves to link the lantern units into the [$Fe^{3+}(H_2O)_2(PO_3OH)$] layer. The details of the linkages between the octahedra and tetrahedra are shown in Fig. 7.

The triple tetrahedral link between the Fe octahedra that forms the [$M_2(TO_4)_3$] (where M represents the octahedral cation and T the tetrahedral cation) lantern units in the camaronesite structure is also found in the structures of the minerals coquimbite and paracoquimbite, [$Fe^{3+}(SO_4)_6(H_2O)_6$]{$Fe^{3+}(H_2O)_6$}$(H_2O)_6$ (Fang and Robinson, 1970; Robinson and Fang, 1971), but in the latter structures the linking tetrahedra are SO_4 groups and there are two successive such triple linkages, resulting in an isolated [$Fe_3(SO_4)_6$] cluster (Hawthorne *et al*., 2000), which we will refer to as a double lantern unit (Fig. 6).

Among synthetic compounds, the [$M_2(TO_4)_3$] lantern unit (although not yet referred to by that name) was first found in the structure of $NaZr_2(PO_4)_3$ by Hagman and Kierkegaard (1968). In this structure the lantern units are linked into a three-dimensional framework. As pointed out by Hong (1976) and Goodenough *et al*. (1976), the Na^+ cations within this framework

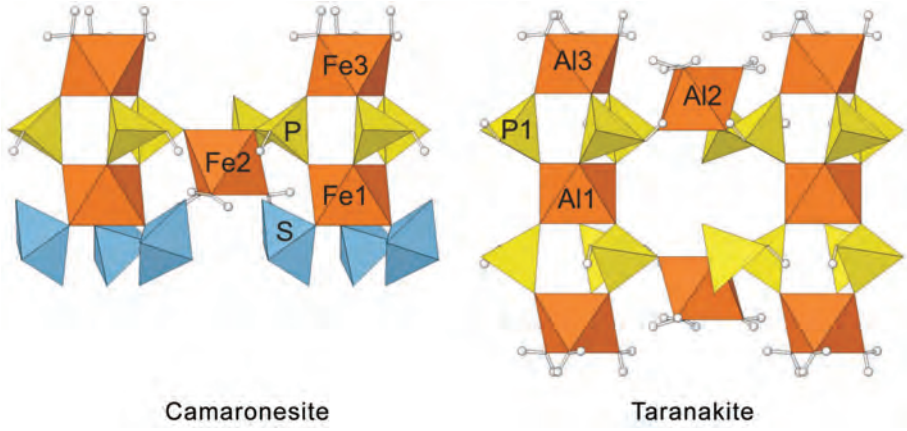

FIG. 7. The polyhedral layers in camaronesite and taranakite viewed on edge with the *c* axis vertical in both cases. Note that for camaronesite both of the half-occupied SO_4 groups sharing the same base are shown.

are mobile, making it a good candidate for fast ion conduction. This insight opened the door to a vast amount of subsequent research into materials with this structure, which has become known as the NASCION (sodium super-ionic conductor) structure (cf. Anantharamulu *et al*., 2011). It is in this research field that the term "lantern unit" for this structural unit has come into common usage (cf. Masquelier *et al*., 2000).

Moore and Araki (1979) reported the structure of $(NH_4)H_8Fe^{3+}_3(PO_4)_6{\cdot}6H_2O$ containing double lantern units, as in the cases of coquimbite and paracoquimbite, but in this case linked into a framework. They conjectured a related structure for the mineral taranakite, $K_3Al_5(PO_3OH)_6(PO_4)_2{\cdot}18H_2O$. They were later proven correct when the structure was finally solved by Dick *et al*. (1998). The structure of taranakite contains $[Al_3(PO_3OH)_6]$ double lantern units, which are linked by additional Al octahedra to form thick corner-sharing polyhedral layers. Even though the lantern units are doubled in the taranakite structure, the linkages within the layers are remarkably similar to those in the polyhedral layers of the camaronesite structure (Figs 7 and 8). The taranakite layer is constructed essentially of two camaronesite layers joined by condensing the lantern units into double lantern units. The linkages and geometries are virtually the same except for the inversion of some polyhedra.

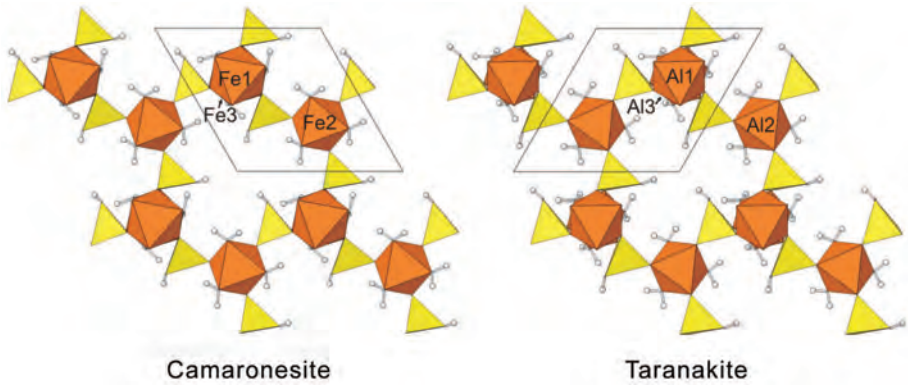

FIG. 8. The $[Fe^{3+}(H_2O)_2(PO_3OH)]$ layer in camaronesite and the corresponding partial layer in taranakite. The view is down **c** in both cases.

The colour of camaronesite

The pale lavender colour of camaronesite is a direct result of the placement of Fe^{3+} in the crystal structure and, in particular, the isolation of each Fe^{3+} octahedron from other Fe^{3+} octahedra by intervening sulfate or phosphate tetrahedra such that no two Fe^{3+} octahedra share a common face, edge or vertex. Similar Fe^{3+} octahedra occur in the phosphate minerals strengite and phosphosiderite and in the sulfate minerals coquimbite and paracoquimbite, all of which share a pale lavender colour. The intervening phosphate and sulfate groups prevent magnetic interactions between the individual Fe^{3+} octahedra that would otherwise produce much more intense colours, such as in the Fe^{3+} minerals hematite, goethite, amarantite and jarosite (Rossman, 1976).

Acknowledgements

Reviewer Giovanni Ferraris and Structures Editor, Peter Leverett, are thanked for their constructive comments on the manuscript. Arturo Molina is thanked for providing specimens of camaronesite. Work at the California Institute of Technology was supported by NSF grant EAR-0947956 and a grant from the Northern California Mineralogical Association. The remainder of this study was funded by the John Jago Trelawney Endowment to the Mineral Sciences Department of the Natural History Museum of Los Angeles County.

References

Anantharamulu, N., Koteswara Rao, K.K., Rambabu, G., Kumar, B.V., Radha, V. and Vithal, M. (2011) A wide-ranging review on Nasicon type materials. *Journal of Materials Science*, **46**, 2821–2837.

Bayliss, P., Kolitsch, U., Nickel, E.H. and Pring, A. (2010) Alunite supergroup: recommended nomenclature. *Mineralogical Magazine*, **74**, 919–927.

Beukes, G.J., Schoch, A.E., Van der Westhuizen, W.A., Bok, L.D.C. and de Bruiyn, H. (1984) Hotsonite, a new hydrated aluminum-phosphate-sulfate from Pofadder, South Africa. *American Mineralogist*, **69**, 979–983.

Brown, I.D. and Altermatt, D. (1985) Bond-valence parameters from a systematic analysis of the inorganic crystal structure database. *Acta Crystallographica*, **B41**, 244–247.

Burla, M.C., Caliandro, R., Camalli, M., Carrozzini, B., Cascarano, G.L., De Caro, L., Giacovazzo, C., Polidori, G. and Spagna, R. (2005) *SIR2004*: an improved tool for crystal structure determination and refinement. *Journal of Applied Crystallography*, **38**, 381–388.

Colombo, F., Rius, J., Pannunzio-Miner, E.V., Pedregosa, J.C., Camí, G.E. and Carbonio, R.E. (2011) *Ab initio* sanjuanite crystal structure solution from laboratory powder diffraction data, complemented by FTIR spectroscopy and DT-TG analyses. *The Canadian Mineralogist*, **49**, 835–847.

de Bruiyn, H., Beukes, G.J., van der Westhuizen, W.A. and Tordiffe, E.A.W. (1989) Unit cell dimensions of the hydrated aluminium phosphate-sulphate minerals sanjuanite, kribergite, and hotsonite. *Mineralogical Magazine*, **53**, 385–386.

Dick, S., Goßner, U., Weiß, A., Robl, C., Großmann, G., Ohms, G. and Zeiske, T. (1998) Taranakite – the mineral with the longest crystallographic axis. *lnorganica Chimica Acta*, **269**, 47–57.

Downs, R.T. (2006) The RRUFF Project: an integrated study of the chemistry, crystallography, Raman and infrared spectroscopy of minerals. In *Program and abstracts of the 19th General Meeting of the International Mineralogical Association in Kobe, Japan*. O03–13.

Fang, J.H. and Robinson, P.D. (1970) Crystal structures and mineral chemistry of hydrated ferric sulfates. I. the crystal structure of coquimbite. *American Mineralogist*, **55**, 1534–1540.

Goodenough, J.B., Hong, H.Y.-P. and Kafalas, J.A. (1976) Fast Na^+ ion transport in skeleton structures. *Materials Research Bulletin*, **11**, 203–220.

Hagman, L.-O. and Kierkegaard, P. (1968) The crystal structure of $NaMe^{IV}_2(PO_4)_3$; Me^{IV} = Ge, Ti, Zr. *Acta Chemica Scandinavica*, **22**, 1822–1832.

Hawthorne, F.C., Krivovichev, S.V. and Burns, P.C. (2000) The crystal chemistry of sulfate minerals. Pp. 1–112 in: *Sulfate Minerals – Crystallography, Geochemistry, and Environmental Signifcance*. Reviews in Mineralogy, **40**. Mineralogical Society of America, Washington, D.C.

Higashi, T. (2001) *ABSCOR*. Rigaku Corporation, Tokyo.

Hong, H.Y.-P. (1976) Crystal structures and crystal chemistry in the system $Na_{1+x}Zr_2Si_xP_{3-x}O_{12}$. *Materials Research Bulletin*, **11**, 173–182.

Mandarino, J.A. (2007) The Gladstone–Dale compatibility of minerals and its use in selecting mineral species for further study. *The Canadian Mineralogist*, **45**, 1307–1324.

Martini, J. (1978) Sasaite, a new phosphate mineral from West Driefontein Cave, Transvaal, South Africa. *Mineralogical Magazine*, **42**, 401–404.

Masquelier, C., Wurm, C., Rodriguez-Carvajal, J., Gaubicher, J. and Nazar, L. (2000) A Powder neutron diffraction investigation of the two rhombohedral NASICON analogues: γ-$Na_3Fe_2(PO_4)_3$ and $Li_3Fe_2(PO_4)_3$. *Chemistry of Materials*, **12**, 525–532.

Mills, S.J., Hatert, F., Nickel, E.H. and Ferraris, G.

(2009) The standardisation of mineral group hierarchies: application to recent nomenclature proposals. *European Journal of Mineralogy*, **21**, 1073–1080.

Mills, S.J., Kampf, A.R., Dini, M. and Molina, A. (2012) Die weltbesten Destinezit-Kristalle und andere seltene Sulfate von Mejillones, Chile. *Mineralien-Welt*, **23**, 73–81.

Mills, S.J., Ma, C. and Birch, W.D. (2011) A contribution to understanding the complex nature of peisleyite. *Mineralogical Magazine*, **75**, 2733–2737.

Moore, P.B. and Araki, T. (1979) Crystal structure of synthetic $(NH_4)H_8Fe_3^{3+}(PO_4)_6{\cdot}6H_2O$. *American Mineralogist*, **64**, 578–592.

Nakamoto, K. (1978) *Infrared and Raman Spectra of Inorganic and Coordination Compounds*, 3rd Edition. Wiley Interscience, New York.

Nash, W.P. (1992) Analysis of oxygen with the electron microprobe: applications to hydrous glass and minerals. *American Mineralogist*, **77**, 453–457.

Peacor, D.R., Rouse, R.C., Coskren, T.D. and Essene, E.J. (1999) Destinezite ("diadochite"), $Fe_2(PO_4)(SO_4)(OH){\cdot}6(H_2O)$: its crystal structure and role as a soil mineral at Alum Cave Bluff, Tennessee. *Clays and Clay Minerals*, **47**, 1–11.

Pouchou, J.-L. and Pichoir, F. (1991) Quantitative analysis of homogeneous or stratified microvolumes applying the model "PAP." Pp. 31–74 in: *Electron Probe Quantitation* (K.F.J. Heinrich and D.E. Newbury, editors). Plenum Press, New York.

Robinson, P.D. and Fang, J.H. (1971) Crystal structures and mineral chemistry of hydrated ferric sulfates. I. the crystal structure of paracoquimbite. *American Mineralogist*, **55**, 1567–1572.

Rossman, G.R. (1976) The optical spectroscopic comparison of the ferric iron tetrameric clusters in amarantite and leucophosphite. *American Mineralogist*, **61**, 933–938.

Salas, R.O. (1964) *Breve informe de una visita realizada a los cateos de sulfato de hierro, en la zona de Cuya, Quebrada de Camarones, Arica*. Instituto de Investigaciones Geológicas, Arica.

Salas, R.O. (1965) *Informe preliminar de la Mina Minerva, Quebrada de Camarones, departamento de Arica*. Instituto de Investigaciones Geológicas, Arica.

Sheldrick, G.M. (2008) A short history of *SHELX*. *Acta Crystallographica*, **A64**, 112–122.